Measurement of the Generator Impedance through the Longitudinal Beam Response Function

N. Towne and J.-M. Wang

National Synchrotron Light Source

Brookhaven National Laboratory,

Upton, NY 11973

(Dated: November 2, 2001)

Abstract

The impedance of a radio-frequency amplifier in a synchrotron storage ring, an amplifier without a circulator, is de-embedded from measurements of the single-bunch longitudinal beam-response function. The presence of both Robinson-mode resonances [N. Towne and J.-M. Wang, Phy. Rev. E **57**(3), p. 3461-7 (1998)] in the response function aids precision in the measurement. The influence of the cavity level-regulation loop is also observed.

I. INTRODUCTION

The National Synchrotron Light Source (NSLS) vacuum-ultraviolet (VUV) ring is unusual in that beam loading of the two radio-frequency (rf) systems is unusually large. In the main rf system, in particular, the beam-loading parameter $Y = 2I_{\rm av}R/V$ exceeds 15, the detuning angle exceeds 86°, and the rf-mode detuning exceeds the damping rate by a factor more than 20 at high current. The transmission line is strongly over coupled to the cavity to the extent that the resonant standing-wave ratio is 5.5. No isolator between the generator and cavity is present although a directional coupler is inserted to damp transmission-line resonances, which reduces the effective beam loading.

The problem of quantifying single-bunch longitudinal dipole modes [1], or Robinson modes [2], requires understanding the highly resonant features of the impedance of the ring with frequencies near revolution harmonics. The rf modes of the cavities in the ring, in particular the accelerating mode of the main cavity, heavily influence the Robinson modes. The problem of characterizing the impedances of these accelerating modes sufficiently well to permit quantitative predictions of the longitudinal beam-response function (LBRF), coherent frequencies, damping rates, and beam-response-function enhancements of noise backgrounds [3] in the NSLS VUV ring over the range of rf-system operating conditions is non-trivial [4].

With such strong coupling of the transmission line and rf amplifier to the cavity, it is necessary to carefully quantify these details in order to characterize the loading of the cavity by the generator and hence the impedance of the cavity as seen by the beam. While elements of the transmission line and its coupling to the cavity are accessible to direct rf measurements, the impedance of the generator, a 50-kW tetrode amplifier, is not directly measurable. This is because cold (no DC power) measurements of its impedance are not useful because the working impedance is dominated by the beam in the tetrode. This tetrode-beam impedance has, due to internal feedback, unknown resistive and reactive components. For this reason the direct measurement of the amplifier impedance as unproductive.

We report here the measurement of the generator impedance by de-embedding it from measurements of the longitudinal beam-response function (LBRF), the response of the beam to an externally applied perturbation of the voltage in the ring seen by the beam, through the use an analytic model that relates the loaded rf-cavity damping rate and detuning to the generator impedance. This analytic model incorporates the details of the transmission

line and its coupling to the cavity.

A feature of the VUV ring is utilized to add precision to the measurement of the generator impedance. The accelerating mode of the main cavity has a damping rate that is small compared to coherent frequencies; as a result, under some conditions, the LBRF shows resonances of both modes of the coupled beam-cavity system (Fig. 1) [1]. These features, providing more structure in the LBRF than is present in rings where the beam couples only weakly to the accelerating mode [5], permit more precision in the determination of the RF system parameters that influence the Robinson modes than would otherwise be possible. In addition, the resulting fits turn out well, providing confidence that the model provides a precise representation of the Robinson modes and the features of the RF system that influence them.

The report proceeds as follows. In section II we define the basic model of the beam and cavity used and give the expressions for the characteristic equation for the complex-valued coherent frequencies and LBRF. Also in this section we describe general features of the loading of the cavity by the power-port and define the forward phase diagnostic since it is used in parameterizing the detuning of the cavity. This section gives the general theoretical framework under which the machine data are analyzed. Section III is VUV specific. In this section we specify the details of the coupling of the cavity to the transmission line and the transmission line itself. Then we give the LBRF data, the fits to these data, the generator impedances extracted, and comment on the quality of the fits.

Table I gives the VUV ring parameters used in most of the calculations.

II. RELATION OF EFFECTIVE CAVITY PARAMETERS TO THE GENERATOR

The purpose of this section is to give the framework under which the machine data are analyzed. In section II A the characteristic equation and longitudinal beam-response function (LBRF), which relate the coherent frequencies and the LBRF to the cavity detuning Δ' and damping rate Γ' of the loaded cavity (i.e., as seen by the beam), are given. In Sec. II B the intrinsic-cavity detuning Δ and damping rate Γ are related to the characteristics of the transmission line, generator, and their coupling to the cavity.

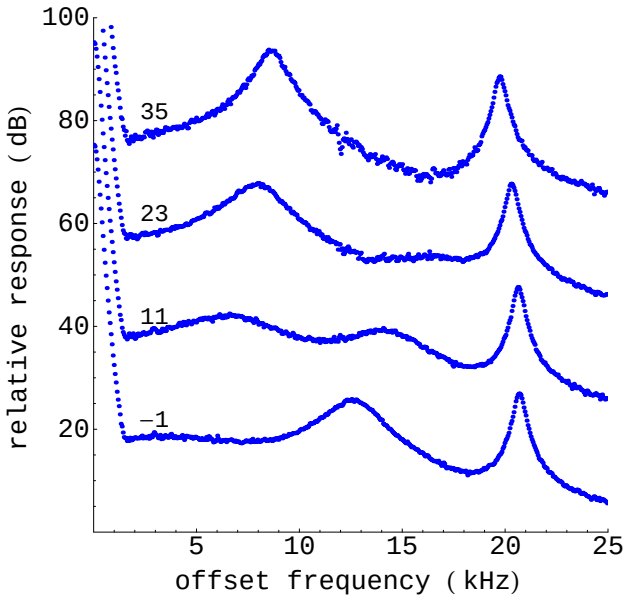

FIG. 1: LBRFs for a single-bunch beam in the NSLS VUV ring. The traces are distinguished by different forward-power-to-cavity-field phases given in the legend (in degrees). Two resonances are visible within 20 kHz offset of the rotation harmonic that are sensitive to the cavity detuning. These are the two Robinson modes [1]. In contrast, the quadrupole-mode resonance at 20 kHz offset is not sensitive to the cavity detuning (more on this in Sec. III B).

A. Characteristic equation and the longitudinal beam-response function

The cavity admittance is modeled as a rational function of the frequency ω using the sign convention of reference [1]:

$$Y_c(\omega) = \frac{1}{R}\left(1 + jQ\left(\frac{\omega}{\omega_r} - \frac{\omega_r}{\omega}\right)\right). \tag{1}$$

In this expression, R is the shunt impedance, Q is the quality factor, ω_r is the resonant frequency of the rf mode, ω_0 is the revolution frequency, the harmonic number h is such that ω_r is near $h\omega_0$, and the damping rate $\Gamma = \omega_r/2Q$. The detuning angle Θ is defined so that $\tan\Theta = Q\,(h\omega_0/\omega_r - \omega_r/h\omega_0)$, and the detuning frequency $\Delta = h\omega_0 - \omega_r$. The approximation $\tan\Theta \cong \Delta/\Gamma$ holds when $\Delta \ll \omega_0$.

When calculating coherent frequencies and the LBRF one must use parameters reflecting the cavity as the beam sees it, i.e., as the cavity is actually resistively and reactively loaded

TABLE I: VUV parameters.

parameter	symbol	value
beam energy	E_0	744 MeV
energy loss per turn	U_0	14.4 keV
momentum compaction	α	0.0245
revolution frequency	ω_0	$2\pi \times 5.8763$ MHz
incoherent synchrotron frequency	ω_s	$2\pi \times 11$ kHz
rf peak voltage	V	80 kV
rf harmonic number	h	9
rf mode normalized impedance	R/Q	125/2 Ω
unloaded Q (including HOM loads)	Q	11,800
unloaded cavity impedance	R	737,500 Ω
input-port standing-wave ratio	κ	5.5
coupling-transformer ratio	n	51.8
coupling-loop inductance	L	90 nH
forward phase	$\Phi_{\rm at}$	variable

by the power port. Primed parameters are used to represent these quantities.

$$Y_c'(\omega) = \frac{1}{R'}\left(1 + jQ'\left(\frac{\omega}{\omega_r'} - \frac{\omega_r'}{\omega}\right)\right). \tag{2}$$

We also have the loaded damping rate $\Gamma' = \omega_r'/2Q'$, the detuning angle $\tan\Theta' = Q'(h\omega_0/\omega_r' - \omega_r'/h\omega_0)$, the detuning frequency $\Delta' = h\omega_0 - \omega_r'$, and the approximation $\tan\Theta' \cong \Delta'/\Gamma'$ when $\Delta' \ll \omega_0$. In terms of these variables, the characteristic equation for the complex-valued coherent frequency Ω is [1]

$$(\Omega^2 - \omega_s^2)(\Omega + \Delta' - j\Gamma')(\Omega - \Delta' - j\Gamma') = -\xi I[\omega_c'(\Omega - \Delta' - j\Gamma') - \omega_c'^*(\Omega + \Delta' - j\Gamma')]\ , \tag{3}$$

where α is the momentum-compaction factor, ω_s is the incoherent synchrotron frequency, $\omega_c' = \Delta' + j\Gamma'$, $\xi = \xi' = e\Gamma R\alpha/T_0E_0$, T_0 is the revolution period, and E_0 is the particle energy. The natural damping rate of the ring is small compared to coherent-mode damping rates of interest and is neglected in this equation.

In practice, coherent frequencies were calculated using the more general discrete-time

version of Eq. (3)

$$(z-2+z^{-1}+T_0^2\omega_s^2)(z-z_c')(z-z_c'^*)=T_0^2\xi Iz\left[j\omega_c'T_0(z-z_c'^*)+(j\omega_c')^*T_0(z-z_c')\right], \qquad (4)$$

where $z = e^{j\Omega T_0}$ relates the complex variables z and Ω and $z_c' = e^{j\omega_c' T_0}$. Equation (4) is derived using the formalism of discrete-time systems [6] and is valid, in principle, for detuning not small compared to ω_0. It is equivalent, for the present purposes, to Eq. (3). Figure 2 gives an example of the behavior of the solutions of Eq. (3) on the complex-Ω plane as a function of beam current.

Now we turn to the LBRF for a sinusoidal voltage of magnitude V_m applied to the beam as a function of the real modulation frequency ω_m. Define the function $z_m = e^{j\omega_m T_0}$ of the externally applied rf frequency ω_m (this is not modulation of the rf). Then the LBRF is the ratio of the phase response φ_m of the beam to the externally applied voltage V_m:

$$\frac{\varphi_m}{V_m}=-\frac{e2\pi\alpha}{E_0}\left[z_m-2+z_m^{-1}+T_0^2\left(\omega_s^2-\xi Iz_m\left(\frac{j\omega_c'T_0}{z_m-z_c'}+\frac{(j\omega_c'T_0)^*}{z_m-z_c'^*}\right)\right)\right]^{-1}. \qquad (5)$$

Figures 3 and 4 give an example of the LBRF for the VUV ring calculated from Eq. (5).

The method by which the primed parameters are calculated from the unprimed parameters and the forward-phase (the phase between the forward wave on the transmission line and the cavity field) diagnostic, which is the application of the formalisms of references [7, 8] to the types of elements present in the VUV ring, is discussed in section II B. This treatment is applied specifically to the VUV ring in section III A.

B. Power-port loading

The impedance of the generator has an effect on synchrotron frequencies because it both pulls the detuning Δ and increases the damping rate Γ of the RF mode. This effect is large in the main cavity of the VUV ring because the high beam loading requires strong coupling of the transmission line to the cavity. For the same reason, the details of the coupling of the generator to the amplifier must be considered when calculating coherent frequencies and beam-response functions through Eq. (3) and Eq. (5), respectively.

In Fig. 5 is shown an equivalent circuit model of the cavity, transmission line, and generator. The model contains the cavity admittance Y_c, an ideal transformer giving the strength n of the coupling of the cavity to the transmission line, a two-by-two admittance matrix Y

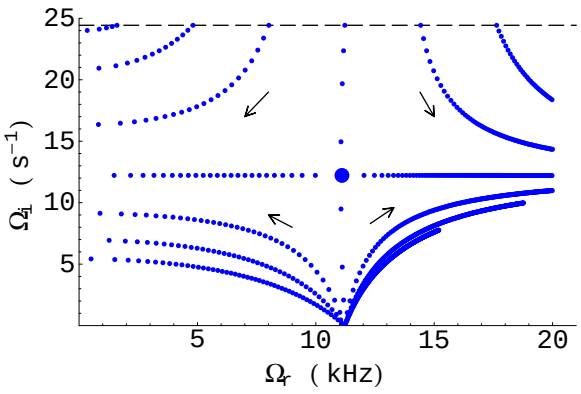

FIG. 2: Solutions of Eq. (4) plotted on the complex Ω (Ω_r, Ω_i) plane as a function of beam current for cavity detuning from $\omega_s/7$ to $13\omega_s/7$ in $2\omega_s/7$ steps. The dashed line is the cavity damping rate Γ'. The zero-current limits of the beam-mode loci are at $\Omega = \omega_s$ on the real axis and of the cavity-mode loci are on the $\Omega_i = \Gamma'$ axis. The large dot at the center of the figure is the beam-mode/cavity-mode collision point at $I = \Gamma'^2\omega_s/2\xi\omega_r'$ and $\Delta' = \omega_s$ [1]. Small dots are given at 10 mA intervals. Arrows give the direction of increasing beam current. The VUV parameters of Table I are used in the calculation.

representing components on the transmission line linking the cavity and generator, and the constant generator admittance Y_g.

The three basic (four scalar) equations

$$I_b - I_c = Y_c V_c \tag{6}$$

$$I_g - I_{\rm TL} = Y_g V_g \tag{7}$$

$$\begin{bmatrix} nI_c \\ I_{\rm TL} \end{bmatrix} = Y \cdot \begin{bmatrix} V_c/n \\ V_g \end{bmatrix} \tag{8}$$

constrain the cavity current I_c, the cavity voltage V_c, the current $I_{\rm TL}$ on the transmission line, the generator voltage V_g, the beam current $I_b = -2I_{\rm av}$, and the generator current I_g. To determine the specific form of Δ' and Γ', one calculates the cavity admittance Y_c' seen by the beam

$$Y_c' = I_b/V_c \mid_{I_g=0} . \tag{9}$$

Trivially, from Eq. (2), $1/R' = \mathrm{Re}[Y_c']$. One can also easily verify that

$$Y_c' R = j \tan\Theta + \chi \tag{10}$$

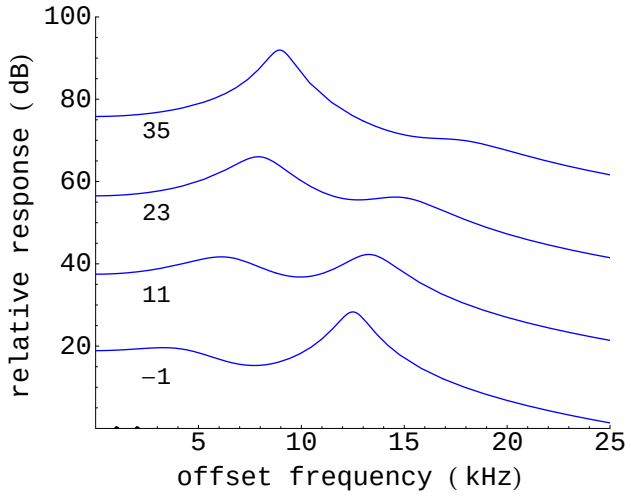

FIG. 3: Magnitude of the LBRF calculated from Eq. (5) for the VUV parameters of Table I, beam current 109 mA, and for four values of the forward phase $\Phi_{\rm at}$ (Sec. II B), in degrees, as given in the legend (positive is capacitively detuned).

for Y_c at the rf frequency, where χ is complex valued and independent of Θ. Then necessarily

$$\frac{\Delta'}{R'\Gamma'} = \frac{\Delta}{R\Gamma} + \frac{\mathrm{Im}[\chi]}{R}. \tag{11}$$

The loss factor of the cavity $k_0 = R\Gamma = R'\Gamma'$ is independent of the loading of the cavity so the loaded detuning Δ' is displaced from the unloaded detuning Δ by the fixed amount:

$$\Delta' = \Delta + \Gamma\,\mathrm{Im}[\chi]. \tag{12}$$

By solving these equations, where Y contains the specifics of the elements in the transmission line between the cavity and the generator, one can determine the total detuning and damping rate of the cavity seen by the beam.

The last thing that needs to be done, before considering the specifics of Y, is to relate the detuning Δ' and damping rate Γ' to the forward-phase diagnostic, since this parameter is measured and, in practice, used to control the cavity detuning Δ. The forward- and reverse-wave complex-valued amplitudes a_g and b_g,

$$\begin{bmatrix} a_g \\ b_g \end{bmatrix} = \frac{1}{2}\begin{bmatrix} 1/\sqrt{Z_0} & \sqrt{Z_0} \\ 1/\sqrt{Z_0} & -\sqrt{Z_0} \end{bmatrix} \cdot \begin{bmatrix} V_g \\ I_{\rm TL} \end{bmatrix}, \tag{13}$$

represent the amplitudes of the forward and reverse traveling waves on the transmission line at the forward-phase pickup. Z_0 is the characteristic impedance of the transmission line and

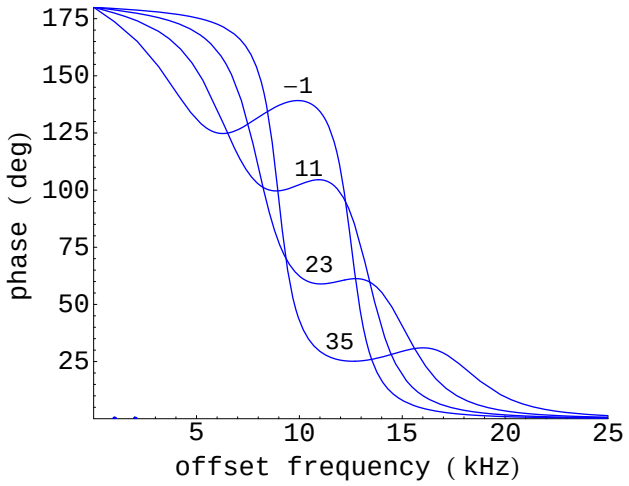

FIG. 4: Phase of the LBRF calculated from Eq. (5) for the VUV parameters of Table I, beam current 109 mA, and for four values of the forward phase $\Phi_{\rm at}$ (Sec. II B), in degrees, as given in the legend (positive is capacitively detuned).

κ is the standing wave ratio of the cavity viewed from the transmission line ($R = n^2 \kappa Z_0$). The forward phase $\Phi_{\rm at}$ is defined as

$$\Phi_{\rm at} = \mathrm{Phase}(a_g/V_c) \tag{14}$$

and is, for the moment, regarded as a function of Δ. Equations 14 and 12 are then inverted to obtain Δ as a function of $\Phi_{\rm at}$.

The exact position of the pickup on the transmission line is immaterial because delays change a_g and b_g only by a phase factor and its inverse, respectively. The calibration of $\Phi_{\rm at}$ is important, however, and is accomplished by assigning the value zero to the phase at which the cavity detuning Δ minimizes the reflection coefficient $|b_g/a_g|$. Thus values from the calibrated forward-phase diagnostic are mapped to the beam-witnessed detuning Δ'.

III. THE GENERATOR IMPEDANCE

In this section we first specify, in Sec. III A, the admittance matrix Y of Eq. (8) specific to the VUV main-cavity rf system. Then, in Sec. III B machine measurements of LBRFs are fitted to Eq. (5) where power-port loading is taken into account. The result of these fits is the generator impedance and cavity voltage for best match. Results are given at different

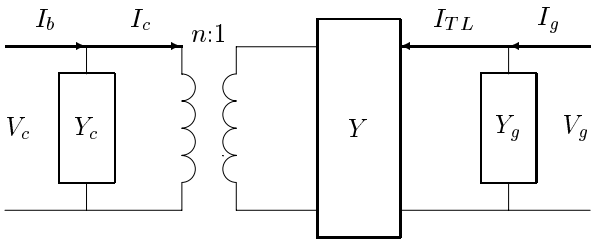

FIG. 5: Equivalent circuit of the cavity and transmission line containing the cavity admittance Y_c, an n:1-ratio ideal transformer, generator admittance Y_g including the transmission-line, cavity and generator voltages V_c and V_g respectively, and the two-by-two admittance matrix Y representing elements between the cavity and the forward-amplitude pickup on the transmission line - but not including the transmission-line delay.

plate currents, the effect of the transmission-line delay is considered, and the quality of the fits are discussed. Ring and RF system parameters used in the fits are given in Table I. Finally, in Sec. III C, results of measurements qualitatively showing the effect on beam-response functions of the one servo loop of the RF system with bandwidth comparable to the coherent frequencies, the loop regulating cavity voltage, are shown.

A. The coupling loop and transmission line

As discussed in section II B, the electrical components between the cavity and the forward-phase pickup are represented, in the model of that section, by the admittance matrix Y. In the VUV ring two components are represented by this matrix. One is the loop that couples the transmission line to the cavity. This coupling loop is characterized by its admittance $Y_L = 1/j\omega L$, where L is the inductance of the loop (Fig. 6). The second is a 10-dB directional coupler used as an attenuator intended to damp transmission-line resonances. The directional coupler is characterized by the its real transmission coefficient T. The length of free transmission line on the cavity side of the forward-phase pickup is immaterial because its only effect is removed later in the calibration of the forward-phase diagnostic measuring $\Phi_{\rm at}$ as discussed in Sec. II B. (The total length *is* relevant to determination of the actual generator impedance and is discussed briefly in Sec. III B).

The specific form of the admittance matrix Y, representing the cavity coupling loop and

10 dB directional coupler and inserted into the solutions of equations 6-8, is

$$Y = \frac{1}{Z_0 + \chi Y_L} \begin{bmatrix} Y_L Z_0 & -2TY_L Z_0 \\ -2TY_L Z_0 & Y_L Z_0 + \chi \end{bmatrix}, \tag{15}$$

where

$$\chi = \frac{1 - T^2}{1 + T^2}. \tag{16}$$

B. Measurements and Results

Each data set taken from the machine consists of LBRFs at four different values of the cavity detuning as measured by four values of the forward phase $\Phi_{\rm at}$, all at similar currents. The amplifier plate current and cavity voltage were recorded for each trace. An example of a data set was shown in Fig. 1 in Sec. I. Both Robinson modes are visible — one varying from 3 kHz to 8 kHz offset from the rotation harmonic and the other visible in the lower three traces at 12 kHz and above from the rotation harmonic. The third trace of the figure shows the condition at which the damping rates of the two modes are about the same — the condition $\Omega_i \simeq \Gamma'/2$ as a consequence of the condition $\mathrm{Im}[\Omega_b] + \mathrm{Im}[\Omega_c] = \Gamma'$, where Ω_b and Ω_c are the two distinct conjugate pairs of complex-valued solutions of Eq. (3) [1]. At the lowest forward phase, 0°, the modes are both stable. Were the forward phase to go negative, the higher-frequency Robinson mode would narrow and eventually go unstable — an expectation consistent with the resistive Robinson-stability criterion.

The other major feature of the data sets and seen in the figure is the quadrupole-mode resonance at 20 kHz offset (roughly twice the synchrotron frequency). This is identified with the quadrupole mode because it has high Q, is insensitive to the detuning but sensitive to the total cavity voltage, and is insensitive to the intensity of the excitation over a broad range. It was once thought to be unstable with sufficient single-bunch current but is now thought to be excited peripherally under these conditions by microwave instability in the turbulent regime.

Measured LBRFs were fit to the calculated LBRF of Eq. (5) as follows.

- Traces were assembled into groups of similar amplifier plate current that are analyzed as a unit. (As a simplifying assumption it is assumed that the generator impedance is a function of the DC plate current only.) The exception to this rule are the data of

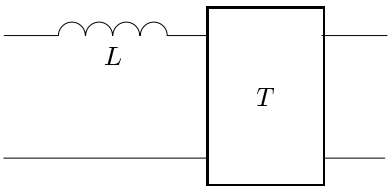

FIG. 6: Equivalent circuit of the two-by-two admittance matrix Y representing elements between the cavity and the forward-wave pickup on the transmission line—but not including delay. L represents the inductance of the coupling loop and T represents the attenuation of a 10-dB directional coupler in the transmission line used to resonances.

section III C where the data sets themselves are analyzed as a unit. In these cases the first (upper) trace of each data set is not used.

- A window in offset frequency over which the spectra are fit is set to exclude the rotation harmonic (at zero offset) and the quadrupole-mode resonance near 20 kHz offset. The result is a 1.6 to 17.1 kHz window.

- The error function is the integrated squares of the differences between the absolute values of the measured and calculated LBRFs (on a linear scale). No phase information was used.

- Although an overall normalization is necessary to accommodate the otherwise unknown gain factors in the measurement, it was also found that a trace-to-trace normalization was necessary. The reason may have to do with variations of bunch length from trace to trace.

- The cavity voltage is measured and recorded for each trace but, as there is some uncertainty in its calibration, an overall calibration factor is used to fit each data set.

- The error function was minimized by varying the complex-valued generator impedance (two parameters) as well as the overall cavity-voltage calibration factor (one parameter).

The first set of five groups of traces was taken at different beam currents between 55 mA and 190 mA and with the amplifier detuning currently used in normal operation. These data are shown in Fig. 7 along with fitted LBRFs.

The second set of five groups of traces are shown in Fig. 8 where the cold (no DC power) amplifier plate-circuit resonant frequency is shifted downward (more capacitively) by 370 kHz. At this setting the cold amplifier tuning remains inductive (above the RF frequency) by 540 kHz. For comparison, the full width of the cold plate-circuit resonance is 1.3 MHz with the output port loaded by 50 Ω. As a result of the more capacitive tuning of the amplifier the beam sees a more capacitively tuned cavity. This means that the higher-frequency (beam) Robinson mode tends to be less evident, the lower-frequency (cavity) Robinson mode is more pronounced, and the fits are better than in Fig. 7.

To see the trends in the data extracted from the fits, in Fig. 9 is plotted, on a Smith chart, the generator impedances extracted from the 10 fits of figures 7 and 8. The effect of the two different amplifier-tuning settings is clearly evident in the two clusterings of data points. Figures 7 and 8 also show fairly good fits between the machine data and the calculated LBRFs.

Up to now the impedance results have reference plane at the start of the transmission line (the inner wall of the cavity). The transmission-line delay and directional coupler are included in the generator impedances of Fig. 9. The transmission-line delay is less than an rf period by 1.93 ns. When these differences are taken out of the generator impedance, one obtains the output impedances of the amplifier alone (Fig. 10). The results show a rather capacitively detuned amplifier. Since the plate circuit is cold tuned inductively, this suggests that feedback within the amplifier has sufficient magnitude and phase to provide capacitive loading of the plate circuit by the tetrode beam. This highlights a limitation of cold tuning an amplifier for Robinson stability.

To summarize, the appearance of both Robinson modes in the beam-response function adds structure to the LBRF that permits sensitive measurement of the generator impedance. Consequently, it is preferable, when using the Robinson-mode LBRF as a diagnostic tool, to operate the RF system in a regime where the two Robinson modes have similar damping rates so that they both provide visible peaks in the LBRF that can be used to fit to the model. But in rings that have RF modes with large damping rates, the two Robinson modes, in a regime in which they are similarly damped, would not be distinguishable because of their large damping rates; precise measurements in such cases may more difficult. In the VUV ring the Robinson-mode LBRF proved suitable to provide considerable information on the main-RF-system generator impedance.

It was hoped that measured LBRFs would tell us the trend in the generator impedance as a function of beam or plate current. Unfortunately it was found that the data do not support such a determination.

C. The cavity-level regulation (ALC) servo loop

Discrepancies in the fits of the previous section, whose origin must be outside of the model used, can be seen, however. A mechanism that modifies the LBRF that is outside of the model used here is the cavity level-regulation servo loop (ALC) used in the RF system. In principle, describing the Robinson modes in a ring with an RF system having feedback control loops requires a description of how the loops interact with the beam motion. This is a complicated subject in itself [9, 10] and it is discussed only qualitatively here. In the VUV ring the feedback loops are generally slow compared to the synchrotron motion and have little effect on the coherent motion. The one exception is the level-regulation loop (ALC) of the main cavity. In this loop the bandwidth is comparable to or greater than the synchrotron frequency and the loop has a marked effect on the Robinson modes. Up to this point data in this paper were taken with the bandwidth of this loop reduced to a fraction of its normal value. In this section we give data showing the impact of the bandwidth of this one feedback loop on the Robinson modes.

A collection of LBRFs with ALC gain at the normal operating condition is shown in Fig. 11. The fits of Fig. 11 are generally poorer than in figures 7 and 8. In Fig. 12 is shown variation of the beam response function with ALC gain. Although the gains were not measured, the general behavior is evident in the figure. As the gain increases, the lower Robinson-mode resonance is pushed upward toward the upper resonance. This behavior is reminiscent of the behavior of the LBRF as the beam current approaches the current at which the collision of the beam and cavity Robinson modes occurs [1]. For the VUV parameters this current is 33 mA (Fig. 2)—considerably below the current of Fig. 12. One might think that the value of the momentum compaction α is in error on the high side. This would have the effect of reducing the factor ξI in Eq. (5) making the current look smaller and moving the peaks together. This is unlikely, however, because measurements of α are not likely to be significantly in error. For this reason it is evident that the model of section II lacking feedback is not adequate to describe these data.

Finally, Fig. 13 shows a Smith-chart plot of the generator impedance from Fig. 11 as well as from Fig. 7. Slightly more scatter is evident in the impedances of Fig. 11 than in that of Fig. 7 consistent with the poorer fits.

IV. CONCLUSION

We described a method for measuring the output impedance of an RF amplifier in a storage ring. The theory, method of analyzing the data, and results when applied to the VUV ring were described. Good agreement between measured and predicted LBRFs were obtained. This has given us confidence both in the applicability of the models for Robinson modes, and for the essential features of the model describing power-port loading and the values of parameters relevant to this model. In general, the results have given us a quantitative description of the Robinson modes in the VUV ring that is more complete and accurate than previously known.

In particular, the generator impedances measured have shown why the Robinson modes are stable and why, when the new amplifier output-coupling loop was installed, the first attempt to fill the ring with the plate tuning more capacitive than is currently used failed. Prior to this study, plate tuning, in an RF system without a circulator, was an entirely empirical adjustment. While it is preferable to have a circulator to reduce interactions between the amplifier and cavity, measurement of the generator impedance has taken some of the guess work out of setting up the amplifier in the absence of a circulator.

Measurements also showed the effect of the cavity level-regulation loop on the Robinson modes and the generator impedance.

This study also showed the utility of intimate coupling of the beam and cavity for the problem of using the LBRF to determine machine parameters. The existence of two resonances with moderate Qs provides additional structure in the LBRF—structure that makes fits of models more difficult and adds precision in the determination of machine parameters when the fits are good.

V. ACKNOWLEDGMENTS

This work was performed under the auspices of the U.S. Department of Energy under contract No. DE-AC02-76CH00016. The analytic-computation package Mathematica [11] was used to solve equations and generate figures.

REFERENCES

[1] N. Towne and J.-M. Wang, Phy. Rev. E **57**(3), 3461 (1998).

[2] K. W. Robinson, *Instabilities in RF Systems* (1964), Cambridge Electron Accelerator Laboratory Report No. CEAL-1010.

[3] R. Biscardi, G. Ramirez, G. P. Williams, and C. Zimba, Rev. Sci. Instrum. **66**, 1856 (1995).

[4] B. C. Craft, in *1985 Particle Accelerator Conference, Vancouver, BC, Canada*, edited by A. Strathdee, TRIUMF (IEEE, Piscataway, NJ, 1985), no. 5 in NS-32, p. 2525.

[5] J. M. Byrd, W. H. Cheng, and F. Zimmermann, Phys. Rev. **E57**, 4706 (1998).

[6] R. Talman, *Analysis of Accelerator Instabilities Using the Formalism of Digital Control Systems* (1990), lecture notes.

[7] A. Gamp, in *1991 CERN/RAL Accelerator School, Oxford, England*, edited by S. Turner, CERN (CERN, Geneva, Switzerland, 1991), pp. 396–415, sec. 2.

[8] W. Broome and J.-M. Wang, *Reactive Robinson Instability in the NSLS X-Ray Ring*, Report No. BNL-62789, National Synchrotron Light Source, Brookhaven National Laboratory, Upton, NY 11973-5000 (1996), secs. 2 and 3.

[9] S. Koscielniak, in *1993 Particle Accelerator Conference, Washington, DC*, edited by S. T. Corneliussen, IEEE and APS (IEEE, Piscataway, NJ, 1993), vol. 5, p. 3506.

[10] F. Pedersen, in *1975 Particle Accelerator Conference, Washington, DC*, edited by J. E. Leiss, NBS (IEEE, Piscataway, NJ, 1975), vol. 22 of *IEEE Trans. Nucl. Sci.*, p. 1906.

[11] *Mathematica ver. 4*, Wolfram Research, Champaign, IL (1998).

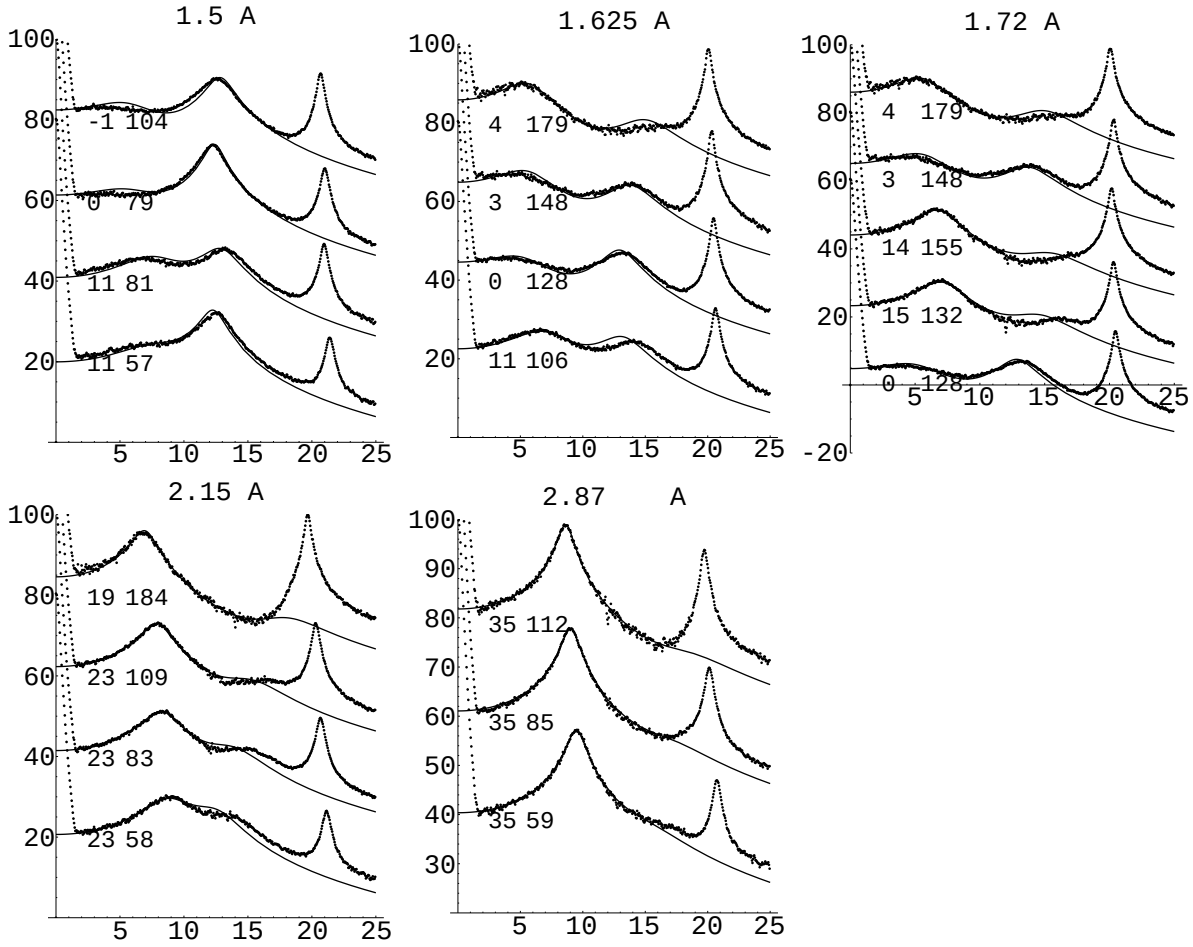

FIG. 7: Measured LBRFs (data points) and calculated (solid lines) least-squares fitted by varying the cavity voltage and the generator impedance. Each plot has grouped traces with similar plate current. The amplifier tuning is approximately that used for normal operation. The horizontal axes are the frequency offsets in kHz and the vertical axes are the relative beam responses in decibels. Each plot is labeled with the average of the plate currents at which the traces were taken and each trace is labeled with the forward phase and beam current at which it was taken.

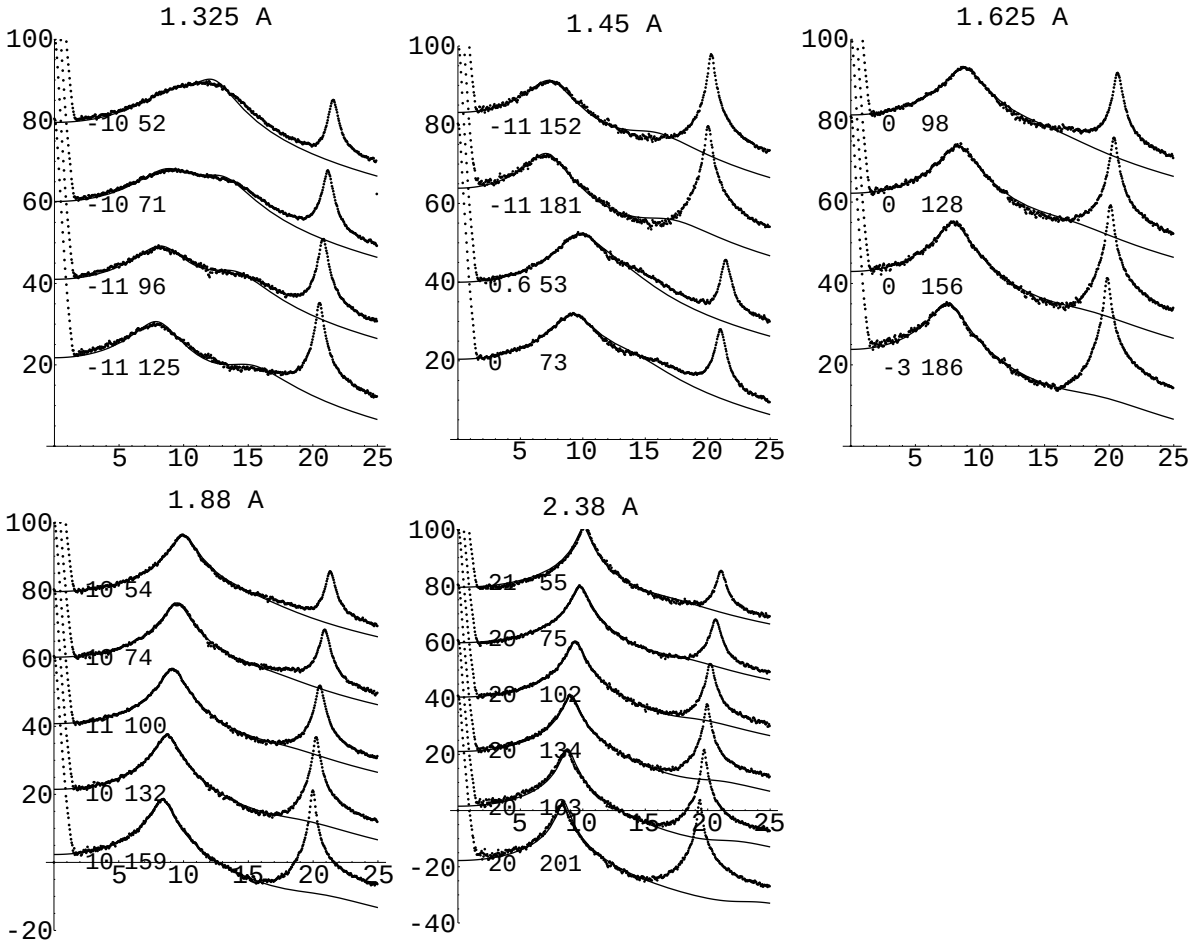

FIG. 8: Measured LBRFs (data points) and calculated (solid lines) least-squares fitted by varying the cavity voltage and the generator impedance. Each plot has grouped traces with similar plate current. The amplifier is detuned capacitively by 370 kHz from that of the previous figure. The horizontal axes are the frequency offsets in kHz and the vertical axes are the relative beam responses in decibels. Each plot is labeled with the average of the plate currents at which the traces were taken and each trace is labeled with the forward phase and beam current at which it was taken.

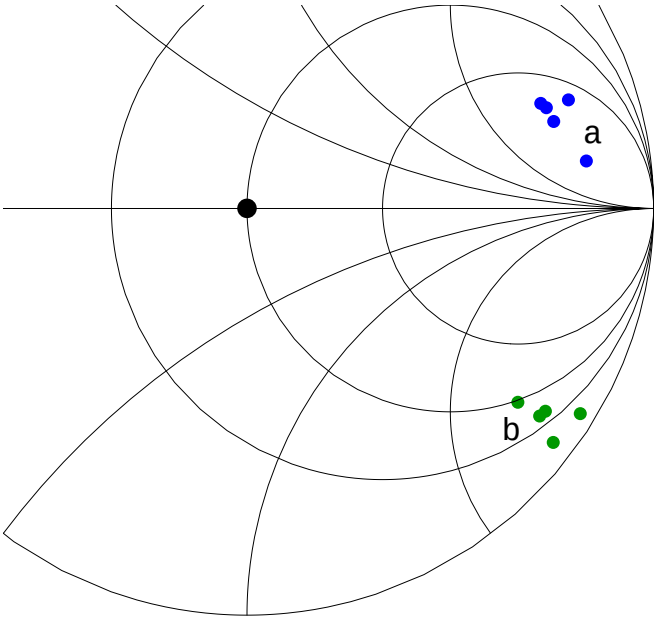

FIG. 9: Smith-chart plot of the generator impedance measurements of Fig. 7 (points 'a' where the amplifier tuning is approximately that used in normal operation) and Fig. 8 (points 'b' where the cold amplifier tune was shifted capacitively by 370 kHz). The large central dot marks the characteristic impedance Z_0 of the transmission line at the origin of the reflection-coefficient plane.

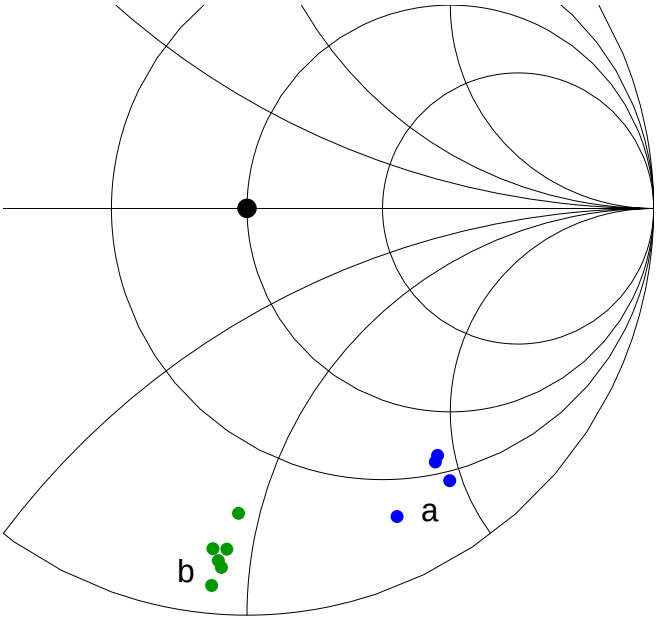

FIG. 10: Smith-chart plot of the amplifier impedance obtained by removing the effect of the transmission line and directional coupler from the data of figure 9. In cluster 'a' the amplifier tuning is approximately that used in normal operation and in cluster 'b' the cold amplifier tune was shifted capacitively by 370 kHz. The large central dot marks the impedance Z_0 (at the reflection-coefficient origin), the characteristic impedance of the transmission line.

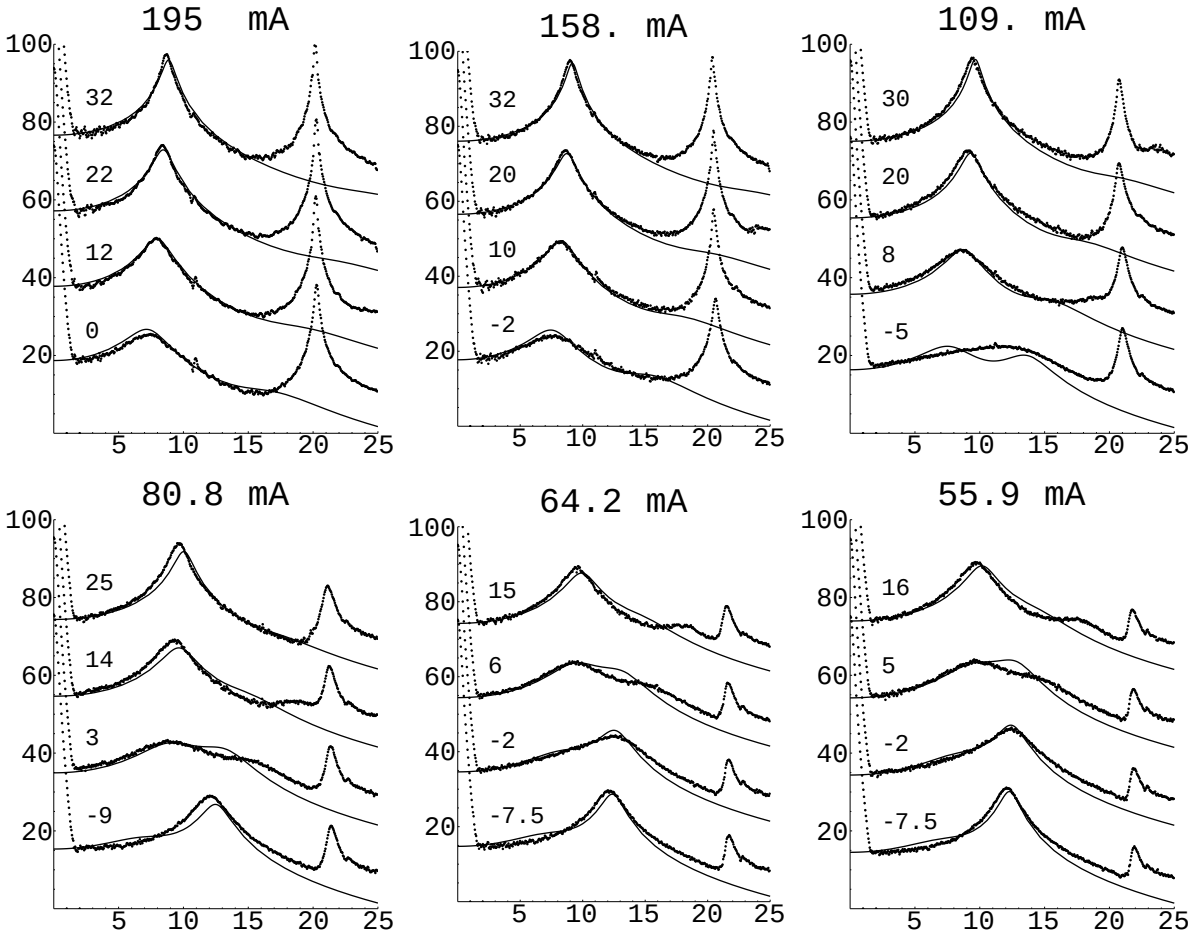

FIG. 11: LBRFs measured (data points) and calculated (solid lines) by least-squares fitting by varying the cavity voltage and the generator impedance. In these data sets the ALC bandwidth had not been reduced and is similar to the synchrotron frequency. The amplifier tuning is approximately the same as is used during normal operation. The beam current is shown in the legend in each plot and, for each trace, the forward phase at the time the trace was taken is shown next to the trace.

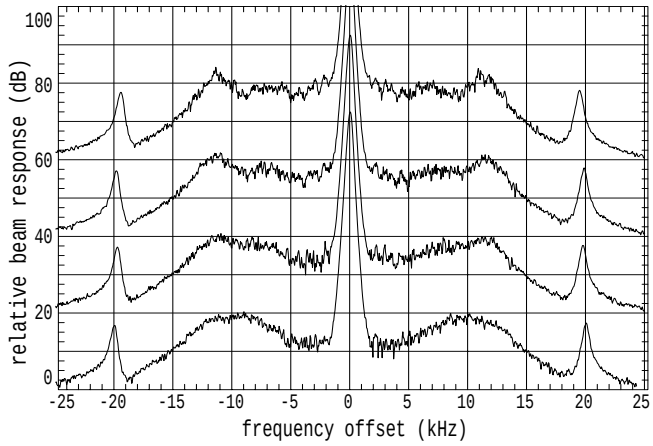

FIG. 12: Variation of the beam-response function as the ALC loop gain is varied. The forward phase is fixed at about 13° and the beam current is 47 mA. The ALC gain is increasing from the top trace to the bottom.

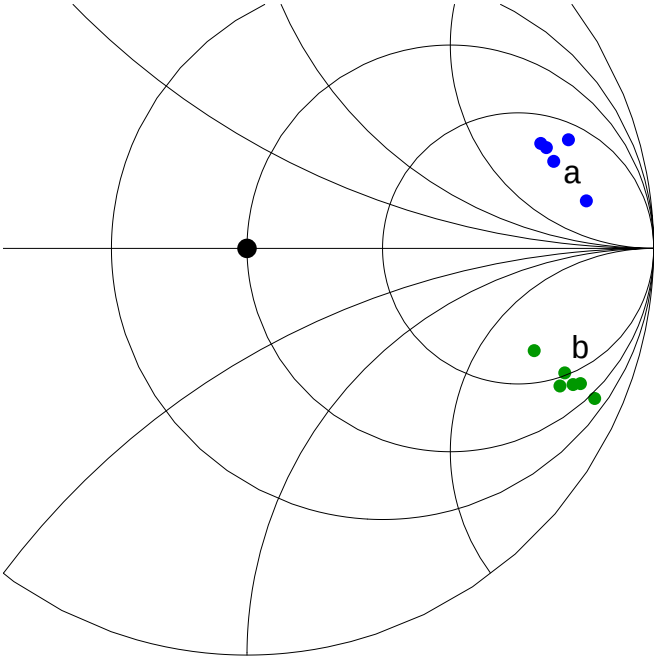

FIG. 13: Smith-chart plot of the generator impedances from Fig. 12 (points 'a' where the ALC bandwidth was reduced to a value small compared to the synchrotron frequency) and 13 (points 'b' where the ALC bandwidth is of order the synchrotron frequency). The large central dot marks the impedance Z_0, the characteristic impedance of the transmission line.